analytical chemistry

Article

pubs.acs.org/ac

Simultaneous Single-Cell Analysis of Na^+, K^+, Ca^{2+}, and Mg^{2+} in Neuron-Like PC-12 Cells in a Microfluidic System

Lu Li, Yuanyuan Fan, Qingling Li, Renjie Sheng, Haibin Si, Juan Fang, Lili Tong, and Bo Tang*

College of Chemistry, Chemical Engineering and Materials Science, Collaborative Innovation Center of Functionalized Probes for Chemical Imaging in Universities of Shandong, Key Laboratory of Molecular and Nano Probes, Ministry of Education, Institute of Molecular and Nano Science, Shandong Normal University, Jinan, Shandong 250014, P. R. China

Supporting Information

ABSTRACT: Various intracellular metal ions have closely related functional roles in the nervous system. An excess or deficiency of essential metal ions can contribute to neurodegenerative diseases. Thus, the detection of various metal ions in neurons is important for diagnosing and monitoring these diseases. In particular, single-cell analysis of multiple metal ions allows us to not only understand the cellular heterogeneity and differentiation but also determine the actual relationships among multiple metal ions in each individual cell. Aiming at the low efficient single-cell manipulation and interference of complex biological matrices within cells in the existing method for single-cell metal ion detection, in this manuscript, we present a convenient, sensitive, and reliable method to simultaneously identify and quantify multiple metal ions at the single-cell level using a microfluidic system. Using the combination of on-chip electrophoresis separation and multicolor fluorescence detection, we achieved the simultaneous analysis of Na^+, K^+, Ca^{2+}, and Mg^{2+} in single PC-12 cells and studied changes in these four metal ions in Aβ_{25-35}-treated PC-12 cells, which is a model of Alzheimer's disease (AD). The data showed that metal ions imbalances in neuron-like cells may be associated with AD induced by Aβ_{25-35}. This method paves the way for multiple metal ion detection in single neuron-like cells, and the results provide insights regarding synergistic function of multiple metal ions in regulation of neurological diseases at the single-cell level.

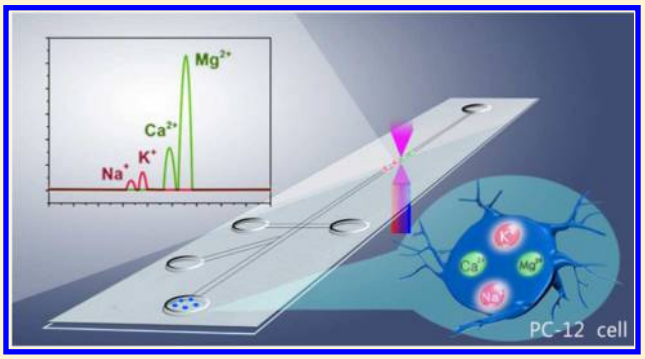

In living organisms, various metal ions have structural and catalytic functions in proteins and enzymes, and they participate in several physiological processes, such as metabolism, antioxidation, signaling, and gene expression.[1−5] In particular, in the nervous system, metal ions play functional roles in neurotransmitter release and transmission, neurite outgrowth regulation, synaptogenesis, and synaptic transmission.[6−10] For example, the intracellular Na^+ concentration can affect the release and reuptake of transmitters.[9] The K^+ released by neurons during this activity must be taken up efficiently to prevent hyperexcitability.[11] As an important signal transduction element, Ca^{2+} in neurons can regulate neurotransmitter release and secretion and then initiate a cascade of signaling events.[8,12] Mg^{2+} is also a key modulator and regulator of neural activity and synaptic plasticity.[10,13] More importantly, in neurons, metal ion concentrations are always closely related, and the ions cooperatively participate in biological events. For example, the intracellular Na^+/K^+ ratio is critical to sustain depolarization of the cell membrane.[14,15] Intracellular Ca^{2+} and Na^+ can influence each other via Na^+-Ca^{2+} exchange, and they have also been reported to both take part in the release of neurotransmitters.[16,17] Additionally, intracellular Mg^{2+} is closely linked to the cellular ionic balance. Mg^{2+} deficiency results in depletion of intracellular K^+ and accumulation of intracellular Na^+ and Ca^{2+} by interfering with ATPase functions.[18] Thus, the maintenance of the homeostasis of multiple metal ions is an important topic for nervous system research. An excess or deficiency of essential metal ions may contribute to neurodegenerative diseases and related neurological disorders including Alzheimer's disease (AD), Parkinson's disease (PD), and Huntington's disease (HD).[19−21]

Thus, the detection and analyses of concentration changes of various metal ions in neurons is an important way to diagnose and monitor neurodegenerative diseases. To detect metal ions, various analytical methods that are based on microscopic, mass spectrometric, and spectroscopic techniques have been widely investigated.[22−24] Qualitative and quantitative data on metal ions could provide information about the cellular biological state and the development of some diseases. However, these methods are usually performed on a number of cells and consequently neglect heterogeneity and differentiation within the population. More importantly, the actual relationship among multiple metal ions in a single cell is concealed by the integrated data from the cell population. If we aim to understand the "story" of the many metal ions in individual

Received: December 20, 2016
Accepted: March 24, 2017
Published: March 24, 2017

DOI: 10.1021/acs.analchem.6b05045
Anal. Chem. 2017, 89, 4559−4565

cells, the simultaneous detection of these metal ions at the single-cell level is one of the most useful methods.

Single-cell metal ion detection has recently been promoted via the use of inductively coupled plasma optical emission spectrometry (ICP-OES), inductively coupled plasma mass spectrometry (ICPMS), and femtosecond laser ionization orthogonal time-of-flight mass spectrometry (fs-LI-OTOFMS).[22,25−28] The major challenge that these techniques face is low efficiency of single-cell manipulation and introduction. In addition, complex biological matrices within cells make it difficult to accurately quantify multiple metal ions in single cells.[28] Although live-cell imaging has exhibited its fascinating ability in monitoring changes in intracellular levels of metal ions, the spectral overlap or cross-talk in the simultaneous detection of multiple molecules is still a critical issue.[29] In addition, it is difficult to provide absolute quantitative information on multiple components by the live cell imaging.[30] Therefore, convenient, sensitive, and reliable methods to identify and quantify multiple metal ions at the single-cell level are still urgently needed.

Microfluidic chips are powerful tools with which to perform single-cell component analyses.[26,31−33] Their microchannel dimensions are ideally comparable to cellular dimensions, and their networks permit accurate cellular manipulation.[34−36] Moreover, a microfluidic chip can be conveniently combined with various detection methods to achieve qualitative and quantitative component analyses.[37,38] In view of the flexibility and applicability of microfluidic chips for single-cell analysis, in this work, we present a new method for simultaneous single-cell analysis of multiple metal ions in a microfluidic system that combines microchip electrophoresis and laser-induced fluorescence detection. Using this microfluidic system, we performed simultaneous quantitative analysis of Na^+, K^+, Ca^{2+}, and Mg^{2+} in single PC-12 cells and investigated the fluctuation of these metal ions in $A\beta_{25-35}$-treated Alzheimer's disease (AD) model cells. The detection process is shown in Scheme 1. Intracellular Na^+, K^+, Ca^{2+}, and Mg^{2+} were derivatized with fluorescent probes. Then, the cells were introduced into the microchip channel one by one and subsequently lysed with a stong electric field. The intracellular contents were separated by microchip electrophoresis in the microchannel. Finally, the multiple fluorescent signals that corresponded to Na^+, K^+, Ca^{2+} and Mg^{2+} were detected in the microfluidic device (MFD). The microfluidic chip enabled convenient single-cell manipulation. Chip electrophoresis effectively separated multiple metal ions in a complex biological system with negligible matrix interference. The treatment of neuron-like cells with $A\beta_{25-35}$ induced various changes in the ion concentrations of intracellular Na^+, K^+, Ca^{2+}, and Mg^{2+}, which implied that an ion imbalance in neuron-like cells may be associated with AD induced by $A\beta_{25-35}$. More importantly, single-cell analyses with our method revealed obvious cellular heterogeneity and an accurate correlation among Na^+, K^+, Ca^{2+}, and Mg^{2+} in each individual PC-12 cell. This method paves a new way for single-cell multiple metal ion analyses, and the results provide insight into the synergistic function of multiple metal ions in regulating neurological diseases at the single-cell level.

Scheme 1. Representation of the Simultaneous Detection of Na^+, K^+, Ca^{2+}, and Mg^{2+} in Single PC-12 Cells Using a Microfluidic System[a]

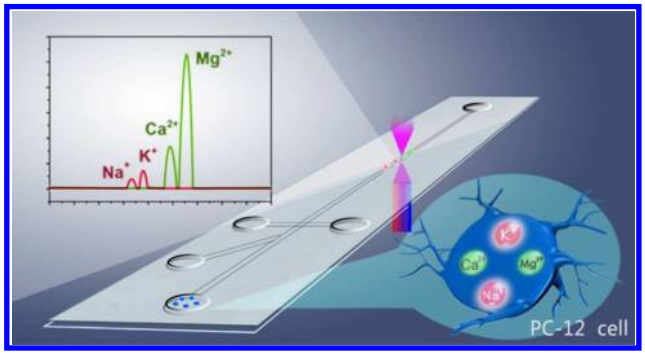

[a]The Na^+, K^+, Ca^{2+}, and Mg^{2+} in the PC-12 cells were first recognized by their fluorescent probes: cBDP, Fluo-3 AM, and Mag-Fluo-4 AM. Then, the cells were injected into a five-reservoir microchip one by one and subsequently lysed with a strong electric field. Next, the metal ions in the cells were separated using microchip electrophoresis in the microchannel. Finally, the multiple fluorescence signals of Na^+, K^+, Ca^{2+}, and Mg^{2+} were detected using MFD.

EXPERIMENTAL SECTION

Reagents and Materials. The Mg^{2+} indicator (Mag-Fluo-4 AM) was purchased from Thermo Fisher Scientific (San Jose, CA, USA). The Ca^{2+} indicator (Fluo-3 AM), cetyltrimethylammonium bromide (CTAB), 3-(4,5-dimethyl-thiazol-2-yl)-2,5-diphenyltetrazolium bromide (MTT), mannitol, pinacidil (K^+ channel opener), and $A\beta_{25-35}$ were acquired from Sigma-Aldrich Chemicals (St. Louis, MO, USA). Sodium chloride (NaCl), potassium chloride (KCl), nifedipine (Ca^{2+} channel antagonist), and 2-amino-2-(hydroxymethyl)-1,3-propanediol (Tris) were obtained from Aladdin Chemical Company (Shanghai, P.R. China). 4′,6-Diamidino-2-phenylindole (DAPI) was purchased from Beyotime Biotechnology (Jiangsu, P.R. China). The Na^+/K^+-ATPase assay kit was purchased from Nanjing Jiancheng Bioengineering Institute (Nanjing, P.R. China). The BODIPY-based fluorescent probe (cBDP) was synthesized in our laboratory.[31] A 5% glucose solution was prepared by dissolving the proper amount of glucose solid in ultrapure water. The electrophoresis buffer (Tris-HCl) was obtained by mixing Tris with the appropriate amount of HCl to adjust the pH. All experimental water was purified with a Sartorius Arium 611 VF system (Sartorius AG, Germany), and all reagents were analytical grade.

Instrumentation. The instrumentation used for the electrophoresis processes include a homemade two-laser excitation and three-channel fluorescence detection system.[32] The instrument is composed of a five reservoirs microchip, programmable four-path-electrode power supply (PFPS), an acquisition system, and a personal computer. We utilized a 10 mW diode-pumped solid-state (DPSS) laser operating at 473 nm to excite the Ca^{2+} and Mg^{2+} fluorescent derivatives and a 15 mW DPSS laser operating at 635 nm to excite the Na^+ and K^+ fluorescent derivatives (CNI Optoelectronics Tech. Co., Ltd., Changchun, China). The fluorescent signals of the Na^+, K^+, Ca^{2+}, and Mg^{2+} derivatives were detected using a R928 photomultiplier (PMT, Hamamatsu, Japan). The collected wavelengths for the Ca^{2+} and Mg^{2+} fluorescent derivatives and the Na^+ and K^+ fluorescent derivatives were 525 ± 15 and 695 ± 15, respectively.

Cell Culture. The PC-12 cell line (rat pheochromocytoma-derived cell line) was obtained from the Type Culture Collection of the Chinese Academy of Sciences (Shanghai, China). The cells were cultured in RPMI 1640 (Hyclone)

DOI: 10.1021/acs.analchem.6b05045
Anal. Chem. 2017, 89, 4559−4565

supplemented with 10% fetal bovine serum (Hyclone) and 1% penicillin−streptomycin (Hyclone) and incubated in a humidified atmosphere with 5% CO_2 and 95% air at 37 °C. Cells were passaged every 2−3 days.

Pretreatment of the Sample. The sample preparation included the standard solution, cellular homogenate, and single cells. For the preparation of the standard solution, 100 μM NaCl and 100 μM KCl were prepared and subsequently mixed with 60 μM cBDP. The cBDP was diluted to 60 μM in 5 mM Tris-HCl (pH 7.4). Additionally, 5 μM of Fluo-3 AM and Mag-Fluo-4 AM were incubated with the cellular homogenate separately at first. Then, the cells were disrupted to obtain the cellular homogenate, and 1 nM $CaCl_2$ and 200 nM $MgCl_2$ were added. The cellular homogenate was prepared using the following method. First, the PC-12 cells were incubated with 60 μM cBDP, 5 μM Fluo-3 AM, and 5 μM Mag-Fluo-4 AM in a 5% glucose solution for 30 min at 37 °C. Then, the cells were disrupted with a BILON92-IIL ultrasonic disintegrator (Shanghai BiLon Materials Inc.), and a suspension of the broken cells was centrifuged (15 000 rpm for 30 min at 4 °C, Sigma 3K 15, Germany) to obtain the supernatant. The cell extract was analyzed immediately. Single cells that were used for the electrophoresis analysis were pretreated as follows. Adherent cells were washed three times with a 5% glucose solution to remove the culture media. Subsequently, the cells were incubated with 60 μM cBDP, 5 μM Fluo-3 AM, and 5 μM Mag-Fluo-4 AM in a 5% glucose solution for 30 min at 37 °C. Next, the cells were washed with a 5% glucose solution to remove the excess probe and then harvested with a 0.25% trypsin-EDTA solution and resuspended in 5 mM Tris-HCl (pH 7.4). For electrophoresis analyses, the cell density was adjusted to 5×10^5 cells/mL.

The Alzheimer's disease model was established as follows. An $A\beta_{25-35}$ stock solution of 1 mM was prepared in deionized water and stored at −20 °C. Then, the solution was preincubated at 37 °C for 5 days to promote aggregation and diluted to the desired concentration with media.[39] Different concentrations of $A\beta_{25-35}$ were added to the PC-12 cells during the logarithmic growth phase and coincubated for 24 h at 37 °C. The excess drug was washed away with PBS three times. Then, the cells were trypsinized and resuspended. Cells with a density of 5×10^5 were used for subsequent testing.

The pinacidil stimulation experiments were performed as previously described.[31] The pinacidil stock solutions (5.0 mM) were dissolved in DMSO, and 5×10^5 cells/mL were incubated with 100 μM pinacidil for 12 h at 37 °C.

The nifedipine was used to block L-type calcium channels. It was dissolved in DMSO first, and 10 μM nifedipine was incubated with 5×10^5 cells/mL PC-12 cells at 37 °C for 12 h.

Detection of Na^+, K^+, Ca^{2+}, and Mg^{2+} on the Microchip. A schematic diagram of the microchip and schematic diagram of single-cell manipulation are shown in Figure S1. First, ultrapure water and 0.1 M NaOH were separately used to rinse the microchannels three times. Then, we injected electrophoresis buffer, 20 mM Tris-HCl (pH 9.0), into the microchannels. The five reservoirs, sample reservoir (S), buffer reservoir (B), buffer waste reservoir (BW), auxiliary reservoir (A), and sample waste reservoir (SW), were filled with 13 μL of electrophoresis buffer. Pre-electrophoresis was performed for 5 min until the baseline was stable. A combination of hydrostatic pressure and electrokinetic gated injection was adopted as the sampling method as described previously.[40] Thirteen μL of cell suspension was injected into reservoir S, and 13 μL of electrophoresis buffer was injected into reservoirs A, B, and BW. Ten μL of electrophoresis buffer was injected into reservoir SW so that variations were formed in the liquid pressure, due to the volume difference, to accomplish the single-cell injection. Next, single-cell loading was achieved by setting the voltage. The voltage applied to reservoir A was 800 V, and 0 V was applied to reservoir BW, while reservoirs SW and B were set as "floating". The voltage output time was 1 s. Finally, the voltage setting was changed to 2500 V for B, 1500 V for SW, 0 V for BW, and "floating" for A to achieve cytolysis and electrophoresis separation. The output time was 100 s.

Cell Viability Assay. To investigate the cytotoxicity of $A\beta_{25-35}$, the MTT test was performed. Confluent PC-12 cells were trypsinized with 0.25% trypsin-EDTA and seeded onto 96-well plates (200 μL, 5×10^5 cells/mL) first. After adherence, the cells were stimulated with various concentrations of $A\beta_{25-35}$ for 24 h and then washed with PBS three times. A 100 μL MTT solution (0.5 mg/mL) was added to each well followed by incubation at 37 °C for 4 h. Subsequently, the supernatant was removed and the formazan crystals were dissolved in 150 μL of DMSO. The absorbance was determined with an RT 6000 microplate reader at 490 nm.

Apoptosis Assay. Cell apoptosis was assessed by analyzing morphologic changes and staining with the DNA-specific fluorescent probe 4′-6-diamidino-2-phenylindole (DAPI). Cells were fixed and permeabilized with 4% paraformaldehyde for 30 min and 0.2% TritonX-100 for 5 min. Then, the cells were stained with DAPI at room temperature for 15 min. A TCS SP5 confocal laser scanning microscope (Leica Co., Ltd. Germany) was used to capture images of the apoptotic cells.

Na^+/K^+-ATPase Assay. The Na^+/K^+-ATPase activity was measured using a Na^+/K^+-ATPase assay kit according to the manufacturer's instructions. In brief, first, a cellular homogenate of 10^7/mL cells was prepared as described above. Then, the protein homogenates were quantified. The absorption at 636 nm was measured using a Hitachi U-3010 UV−vis spectrometer. The Na^+/K^+-ATPase activity was calculated according to a formula.

RESULTS AND DISCUSSION

Fluorescent Detection of Na^+, K^+, Ca^{2+}, and Mg^{2+} Using the Microfluidic System. For fluorescence labeling of the different metal ions, we made a BODIPY-based cBDP probe and reacted this with Na^+ and K^+ to produce fluorescent signals, both with a maximum emission at 675 nm (λ_{ex} = 630 nm).[31] However, Ca^{2+}-sensitive Fluo-3 acetoxymethyl ester (Fluo-3-AM) and Mg^{2+}-sensitive Fluo-4 acetoxymethyl ester (Mag-Fluo-4 AM) can respond to intracellular Ca^{2+} and Mg^{2+} only after the hydrolysis of acetoxymethyl ester via intracellular esterases,[41,42] resulting in fluorescence emission with maximum emissions at 527 and 515 nm, respectively. The reactions between the fluorescent probes and the four metal ions are shown in Figure S2. The excitation and emission spectra of the fluorescent products are shown in Figure S3.

First, we individually detected Na^+, K^+, Ca^{2+}, and Mg^{2+} in a standard solution using the microfluidic system to verify the fluorescent responses of the probes to the metal ions and their migration times in the microchip during electrophoresis. The fluorescent signals of Na^+ and K^+ in the standard solution were directly detected within the wavelength range of 675−705 nm after the solution had been mixed with the cBDP probes. However, Ca^{2+} and Mg^{2+} were detected within the wavelength range of 510−540 nm in the cellular homogenate, which was

DOI: 10.1021/acs.analchem.6b05045
Anal. Chem. 2017, 89, 4559−4565

obtained via lysis of the PC-12 cells after incubation with Mag-Fluo-4 AM and Fluo-3 AM. The respective electropherograms of the four metal ions are shown in Figure 1. We obtained good

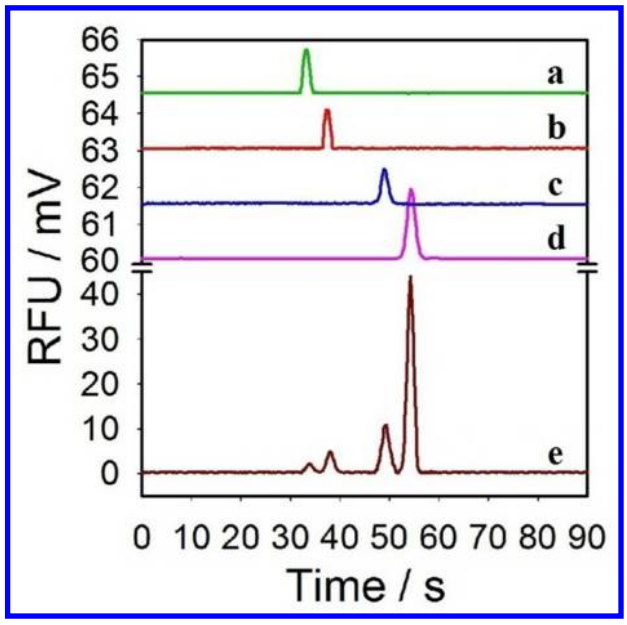

Figure 1. Electropherograms of the fluorescent derivatives of K^+, Na^+, Ca^{2+}, and Mg^{2+} in the standard solution and cellular homogenate. From top to bottom: a, Na^+-cBDP in the standard solution containing 100 μM NaCl; b, K^+-cBDP in the standard solution containing 100 μM KCl; c, Ca^{2+}-Fluo-3 AM in the cellular homogenate added to 1 nM $CaCl_2$; d, Mg^{2+}-Mag-Fluo-4 AM in the cellular homogenate added to 200 nM $MgCl_2$; e, the four fluorescent derivatives in the cellular homogenate (5×10^5 cells). The concentrations of cBDP, Fluo-3 AM, and Mag-Fluo-4 were 60, 5, and 5 μM, respectively.

fluorescent responses from the metal ions. The migration times of Na^+, K^+, Ca^{2+}, and Mg^{2+} were 35, 38, 50, and 54 s, respectively. Good reproducibility was confirmed by relative standard deviations (RSDs) of 0.6%, 0.53%, 0.72%, and 0.68% for Na^+, K^+, Ca^{2+}, and Mg^{2+}, respectively, according to 11 migration time measurements. For quantitation of the metal ions using the microchip system, Na^+, K^+, Ca^{2+}, and Mg^{2+} of different concentrations were detected. The fluorescent signal intensities (peak areas) linearly increased with the concentrations of the metal ions in a certain range. The analytical parameters of this method, such as the linear range, limit of detection (LOD), and reproducibility, are shown in Table S2. The calculated mass LODs for Na^+, K^+, Ca^{2+}, and Mg^{2+} were 0.293 fmol, 0.316 fmol, 0.158, amol and 3.16 amol, respectively, based on an injection volume of 206 pL. The injection volume was obtained by calculating a loaded volume of standard R6G solution in the separation microchannel when the homogeneous detection of R6G solution was performed by the single-cell sampling method described in the Experimental Section.

Signal interference and spectral overlapping of multiple target molecules are the most problematic issues for multicolor fluorescence detection. For the simultaneous detection of Na^+, K^+, Ca^{2+}, and Mg^{2+}, the selectivity of the three probes was investigated to evaluate the interference from other metal ions. The results shown in Figure S4 confirmed that the cBDP probe had good selectivity for Na^+ and K^+, but it could not distinguish Na^+ and K^+ from each other. The Mg^{2+} probe, Mag-Fluo-4 AM, generated some response to Ca^{2+} and Zn^{2+}. Mg^{2+} also caused signal increases for the Ca^{2+} probe Fluo-3 AM. In addition, Na^+ and K^+ had the same emission spectra with large spectral overlapping between Ca^{2+} and Mg^{2+}. Using our method, fluorescent detection was based on microchip electrophoresis, which could effectively separate multiple components in a complex system using the difference in the charge-to-mass ratio. Thus, this method not only allows high-performance splitting of the overlapped spectra of Na^+ and K^+ as well as Ca^{2+} and Mg^{2+} but also eliminates interfering signals from other substances based on their different migration times. In our method, to obtain good separation, 20 mM of Tris-HCl buffer (pH 9.0) containing 20 mM mannitol and a separation electric field of 440 V/cm were selected for on-chip electrophoresis. Next, we simultaneously detected intracellular Na^+, K^+, Ca^{2+}, and Mg^{2+} in the PC-12 cellular homogenate to evaluate the ability of this method to provide good separation and low intereference, for the multiple metal ions detection. After microchip electrophoresis and dual-color fluorescent detection, we obtained four peaks that were completely separated. Using the migration times, each peak was identified as its corresponding metal ion. The resolution between Na^+ and K^+ and between Ca^{2+} and Mg^{2+} was calculated to be 2.4 and 2.1, respectively, indicating a complete separation. Thus, spectral overlapping in fluorescence detection was no longer an issue for this method due to effective electrophoresis separation. In addition, no other peaks appeared in the electropherogram of the cellular homogenate, demonstrating that complex biological matrices within cells did not interfere with the detection of the target metal ions. To quantify the four metal ions in the cellular homogenate, the fluorescence intensities of the four metal ions with different concentrations (Na^+, 0.008−2 mM; K^+, 0.008−2 mM; Ca^{2+}, 0.005−0.1 μM; Mg^{2+}, 0.1−60 μM) were measured and calibration curves with the peak areas as *Y*-axis and the concentrations of the metal ions as *X*-axis were obtained (Figure S5). After the fluorescence signals of the four metal ions in cellular homogenate were measured, the four metal ions concentrations were quantified according to a linear equation (Table S2) from the calibration curves. The calculated average concentrations of Na^+, K^+, Ca^{2+}, and Mg^{2+} in the PC-12 cells were 22.36 mM, 115.32 mM, 0.9098 mM, and 0.1153 μM.

Simultaneous Detection of Na^+, K^+, Ca^{2+}, and Mg^{2+} in Single PC-12 Cells. To illustrate the applicability of this method to single-cell metallomics, we simultaneously detected intracellular Na^+, K^+, Ca^{2+}, and Mg^{2+} in single PC-12 cells. After consecutive single-cell sampling, loading, cytolysis, and electrophoretic separation on the microchip, four completely separated peaks from each cell were obtained via dual-channel fluorescent detection. Typical electropherograms from 10 individual PC-12 cells are shown in Figure 2. These peaks were separately identified as Na^+, K^+, Ca^{2+}, and Mg^{2+} based on their individual migration times. Due to the cellular heterogeneity, it may take different times for individual cells to be lysed. The repeatability of the migration times of the four metal ions in single cells was investigated. The RSDs of migration time of Na^+, K^+, Ca^{2+}, and Mg^{2+} in single cells were calculated to be 0.3733%, 0.2328%, 0.3923%, and 0.3882%, respectively. There are no obvious differences in the migration times, indicating a good repeatability.

To further demonstrate the reliability of this method, we used pinacidil and nifedipine, an activator of a K^+ channel and a Ca^{2+} antagonist,[43,44] respectively, to treat the PC-12 cells to induce intracellular ion concentration changes. As the literature describes, pinacidil acts as a K^+ channel opener to regulate the

DOI: 10.1021/acs.analchem.6b05045
Anal. Chem. 2017, 89, 4559−4565

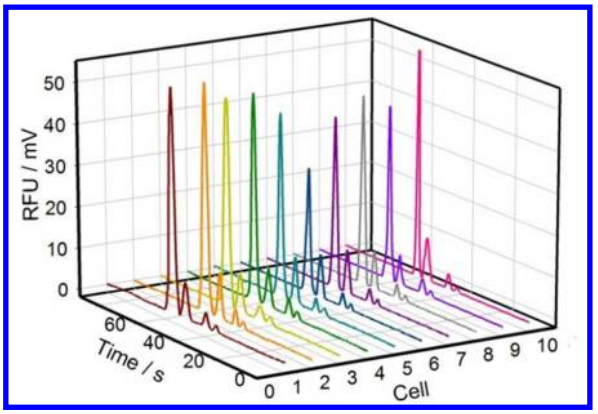

Figure 2. Typical electropherograms from 10 individual PC-12 cells. The cells were incubated with 60 μM cBDP, 5 μM Fluo-3 AM, and 5 μM Mag-Fluo-4 AM. The electropherograms were obtained under the same electrophoresis conditions as in Figure 1.

flow of intracellular K^+ and then induce a decrease in intracellular K^+.[45] The opening of the K^+ channel by the hyperpolarizing drug, pinacidil, can also reduce the intracellular Ca^{2+} influx via voltage-gated channels.[46] Nifedipine, an L-type channel blocker of Ca^{2+}, can specifically block high-voltage-activated (L-type) calcium channels by decreasing their open-state probability. Then, nifedipine can inhibit the Ca^{2+} influx into the cell from extracellular sources. We performed the simultaneous detection of Na^+, K^+, Ca^{2+}, and Mg^{2+} in single cells. The concentrations of Na^+, K^+, Ca^{2+}, and Mg^{2+} in 100 individual untreated PC-12 cells, 100 pinacidil-treated PC-12 cells, and 100 nifedipine-treated PC-12 cells were calculated according to the linear equation in Table S2. The detailed information regarding the qualification of four metal ions in single cells is described in the Supporting Information. Figure 3A shows the individual concentrations of Na^+, K^+, Ca^{2+}, and Mg^{2+} in 50 untreated PC-12 cells, 50 pinacidil-treated PC-12 cells, and 50 nifedipine-treated PC-12 cells. Each column in this figure represents one cell. The four differently shaped points on the same vertical dotted lines represent the Na^+, K^+, Ca^{2+}, and Mg^{2+} in one cell. The statistical data for 100 cells are shown in Figures 3B and S6. The averaged concentrations of Na^+, K^+, Ca^{2+}, and Mg^{2+} in untreated single PC-12 cells were calculated to be 21.07 mM, 122.2 mM, 0.8907 mM, and 0.1062 μM, which are in agreement with the previously reported results.[47−50] In all three groups, the concentrations of Na^+, K^+, Ca^{2+}, and Mg^{2+} display obvious fluctuations, indicating cellular heterogeneity. With the Shapiro-Wilk test, we see that all the concentrations of the four metal ions at pretreatment and post-treatment obey the normal distribution. The *P*-values are all greater than 0.05, which are given in Table S3. In addition, the pinacidil-treated PC-12 cells exhibited different decreases in their K^+ and Ca^{2+} concentrations, which were 46.77% and 31.34% lower, respectively, than those in untreated PC-12 cells on average. Nifedipine-treated PC-12 cells exhibited an intracellular Ca^{2+} decrease that was 30.44% lower than that in untreated PC-12 cells. These significant differences were identified by the two-sample *t* test with *P*-values less than 0.05. The results from our experiment further verified the mechanisms of pinacidil and nifedipine. This demonstration represents one application of our method for multiple metal ion detection. Our results revealed the simultaneous changes in multiple metal ions after drug stimulation at the single-cell level.

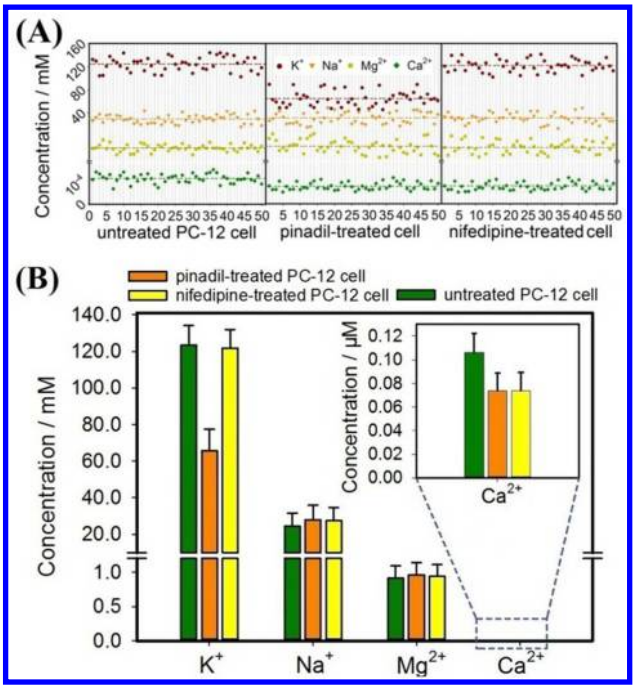

Figure 3. (A) The concentrations of Na^+, K^+, Ca^{2+}, and Mg^{2+} in 50 individual untreated PC-12 cells (left), pinacidil-treated PC-12 cells (middle), and nifedipine-treated PC-12 cells (right). Each column in this figure represents one cell. The four different shaped points on the same vertical dotted lines represent Na^+, K^+, Ca^{2+}, and Mg^{2+} in one cell. The horizontal dotted lines represent the average concentrations of Na^+, K^+, Ca^{2+}, and Mg^{2+} in 50 cells. (B) Average concentration of the four ions in untreated cells (green), pinacidil-treated PC-12 cells (orange), and nifedipine-treated PC-12 cells (yellow). The statistical data were calculated on the basis of 100 cells.

Single-Cell Analysis of the Changes in Na^+, K^+, Ca^{2+}, and Mg^{2+} in Aβ_{25-35}-Treated AD Model Cells. An excess or deficiency in essential metal ions can contribute to neurological disorders.[51] Neurodegenerative diseases may be characterized by abnormal intracellular metal ion levels. In this study, we simultaneously detected Na^+, K^+, Ca^{2+}, and Mg^{2+} in Aβ_{25-35}-treated PC-12 cells and untreated PC-12 cells at the single-cell level to accurately evaluate changes in Na^+, K^+, Ca^{2+}, and Mg^{2+} during Alzheimer's disease (AD). AD is the most prevalent form of dementia.[52] As a neurodegenerative disorder, one obvious characteristic of AD is the presence of senile plaques that are predominantly composed of amyloid beta peptide (Aβ).[53] In our experiment, a smaller 11-amino acid fragment of the full-length peptide, Aβ_{25-35}, was chosen as a convenient stimulant to induce PC-12 cells to become AD model cells because of the similar toxicological properties of this peptide to the native full-length peptide.[54] To optimize the Aβ_{25-35} concentration, we performed a cell viability assay and observed the morphologic changes of the PC-12 cells after treatment with Aβ_{25-35} at different concentrations for 24 h. Finally, 20 μM of Aβ_{25-35} was selected for subsequent experiments because of its obvious cytotoxicity but reduced cell mortality (Figure S7). Next, using the microfluidic system, free Na^+, K^+, Ca^{2+}, and Mg^{2+} in the single PC-12 cells and Aβ_{25-35}-treated PC-12 cells were quantified. The concentrations of the four ions in every cell are shown in Figure S8. The concentration distribution profiles of Na^+, K^+, Ca^{2+}, and Mg^{2+} in 100 PC-12 cells and in 100 Aβ_{25-35}-treated PC-12 cells are shown in Figure 4A. The bar graph in Figure 4B represents the average concentrations of

DOI: 10.1021/acs.analchem.6b05045
Anal. Chem. 2017, 89, 4559−4565

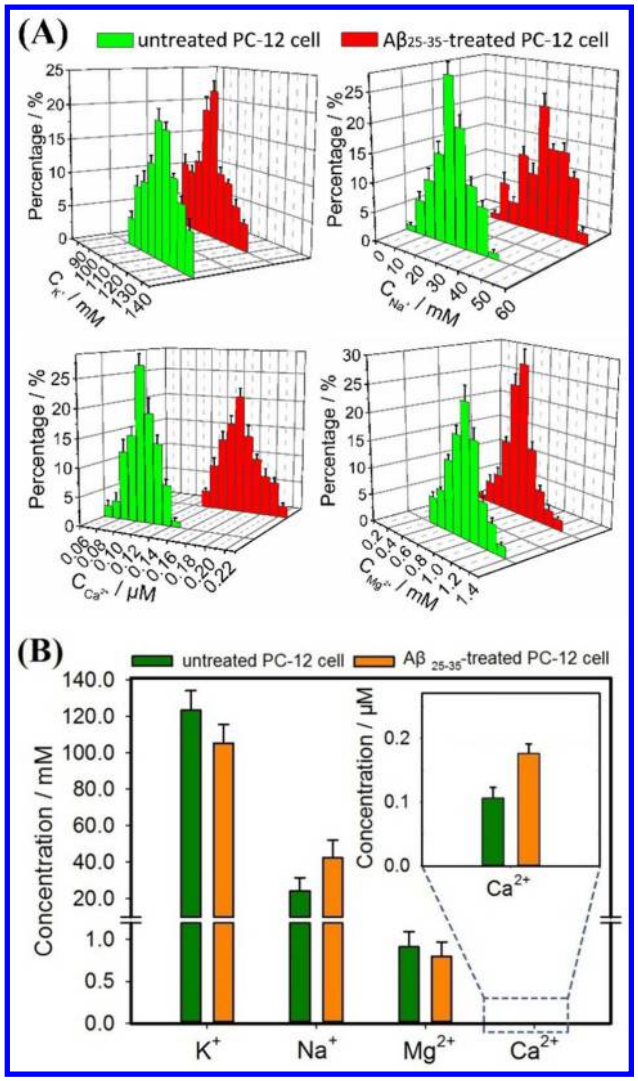

Figure 4. (A) The concentration distribution profile of Na^+, K^+, Ca^{2+}, and Mg^{2+} for 100 untreated PC-12 cells (green) and 100 Aβ_{25-35}-treated PC-12 cells (red). It shows the percentage of cells with different concentrations. (B) The average concentrations of the four ions in untreated (green) PC-12 cells and Aβ_{25-35}-treated PC-12 cells (orange). The statistical data are calculated on the basis of 100 cells.

the four ions in the two groups. On the basis of these data, we observed cell-to-cell variability for the free metal ions among the single cells. We also observed heterogeneity among the PC-12 cells in the Aβ_{25-35}-induced pathogenesis of AD. In addition, the four metal ions in untreated PC-12 cells and Aβ_{25-35}-treated PC-12 cells obey the normal distribution by the Shapiro-Wilk test with the *P*-values all greater than 0.05 (Table S3). An average 0.147-fold and 0.122-fold decrease in the intracellular K^+ and Mg^{2+} and an average 0.647-fold and 0.662-fold increase in the Na^+ and Ca^{2+} was obtained, respectively. By the two-sample *t* test, the significant differences were identified with both *P*-values less than 0.05. We further analyzed the reason for the concentration changes in the intracellular Na^+, K^+, Ca^{2+}, and Mg^{2+} after Aβ_{25-35} treatment. The decrease in K^+ and increase in Na^+ were likely due to the suppression of Na^+/K^+-ATPase activity and induction of apoptosis by Aβ_{25-35}. Na^+/K^+-ATPase plays a crucial role in maintaining the Na^+ and K^+ gradient across the plasma membrane via transporting three Na^+ ions out of the cell and two K^+ ions into the cell by hydrolyzing ATP.[55] Na^+/K^+-ATPase activity was studied using a Na^+/K^+-ATPase assay kit and a UV−vis spectrometer. The Na^+/K^+-ATPase activity was significantly reduced following exposure to Aβ_{25-35} (Figure S9). The reduced Na^+/K^+-ATPase activity was able to inhibit the Na^+ outflow and the K^+ influx, leading to decreased K^+ and increased Na^+. In addition, cell apoptosis is closely related to Na^+/K^+ ionic imbalance.[56,57] We observed the apoptosis of PC-12 cells after treatment with 20 μM Aβ_{25-35} for 24 h (Figure S10). Apoptosis was likely another reason for the ionic reversal (the decrease in intracellular K^+ and increase in intracellular Na^+). The increase in intracellular Ca^{2+} may be due to the formation of an ion channel via the insertion of Aβ into the membrane in a structural configuration, which has been observed in previous reports.[58,59] Additionally, a high intracellular sodium concentration may cause the release of calcium from mitochondria by stimulating Na^+/Ca^{2+} exchange.[18] Changes in Mg^{2+} concentration are closely associated with changes in the concentration of other ions. Mg^{2+} is negatively correlated with cellular Ca^{2+}.[60] When the Ca^{2+} concentration increases, Mg^{2+} concentrations are reduced.[61]

CONCLUSIONS

Herein, we presented a new method for single-cell analysis of multiple metal ions, using a microfluidic system, that combines microchip electrophoresis separation and multicolor fluorescent detection. The method is convenient, sensitive, and reliable for performing single-cell manipulation and simultaneous detection of multiple metal ions. Using this method, we simultaneously analyzed Na^+, K^+, Ca^{2+}, and Mg^{2+} levels in single PC-12 cells and studied the concentration changes in these four metal ions in the AD model of Aβ_{25-35}-treated cells. We obtained accurate concentration changes for the four metal ions in single cells. We observed a metal ions imbalance in Aβ_{25-35}-treated PC-12 cells. The results provide insights into the synergistic function of multiple metal ions in regulating neurological diseases at the single-cell level. This method paves the new way for the simultaneous analysis of other metal ions at the single-cell level.

ASSOCIATED CONTENT

Supporting Information

The Supporting Information is available free of charge on the ACS Publications website at DOI: 10.1021/acs.analchem.6b05045.

Sampling process; fluorescent probe reactions; excitation and emission spectra; selectivity of fluorescent probes; analytical performance of the proposed method; concentration distribution profile; cell viability; concentrations of ions; *P*-value calculated from the Shapiro-Wilk test; Na^+/K^+-ATPase activity assay; apoptosis assay (PDF)

AUTHOR INFORMATION

Corresponding Author

*E-mail: tangb@sdnu.edu.cn. Fax: 86-531-86180017.

ORCID

Bo Tang: 0000-0002-8712-7025

Notes

The authors declare no competing financial interest.

DOI: 10.1021/acs.analchem.6b05045
Anal. Chem. 2017, 89, 4559−4565

■ ACKNOWLEDGMENTS

This work was supported by 973 Program (2013CB933800), National Natural Science Foundation of China (21535004, 21390411, 21675104, and 21675102), and Natural Science Foundation of Shandong Province of China (ZR2016JL008, ZR2016BM02).

■ REFERENCES

(1) Szpunar, J. *Anal. Bioanal. Chem.* **2004**, *378*, 54−56.
(2) Hwang, K.; Wu, P.; Kim, T.; Lei, L.; Tian, S.; Wang, Y.; Lu, Y. *Angew. Chem., Int. Ed.* **2014**, *53*, 13798−13802.
(3) Shi, B.; Su, Y.; Zhang, L.; Huang, M.; Liu, R.; Zhao, S. *ACS Appl. Mater. Interfaces* **2016**, *8*, 10717−10725.
(4) Clapham, D. E. *Cell* **2007**, *131*, 1047−1058.
(5) Hentze, M. W.; Muckenthaler, M. U.; Galy, B.; Camaschella, C. *Cell* **2010**, *142*, 24−38.
(6) Clapham, D. E. *Cell* **1995**, *80*, 259−268.
(7) Mattson, M. P. *Aging Cell* **2007**, *6*, 337−350.
(8) Zhang, Z.; Zhao, L.; Lin, Y.; Yu, P.; Mao, L. *Anal. Chem.* **2010**, *82*, 9885−9891.
(9) Rose, C. R.; Ransom, B. R. *Glia.* **1997**, *20*, 299−307.
(10) Yamanaka, R.; Shindo, Y.; Karube, T.; Hotta, K.; Suzuki, K.; Oka, K. *Neuroscience* **2015**, *310*, 731−741.
(11) Sibille, J.; Dao Duc, K.; Holcman, D.; Rouach, N. *PLoS Comput. Biol.* **2015**, *11*, e1004137.
(12) Burdette, S. C.; Lippard, S. J. *Proc. Natl. Acad. Sci. U. S. A.* **2003**, *100*, 3605−3610.
(13) Palacios-Prado, N.; Chapuis, S.; Panjkovich, A.; Fregeac, J.; Nagy, J. I.; Bukauskas, F. F. *Nat. Commun.* **2014**, *5*, 4667−4667.
(14) Cone, C. D. *J. Theor. Biol.* **1971**, *30*, 151−181.
(15) Nagy, I. Z.; Lustyik, G.; Nagy, V. Z.; Zarándi, B.; Bertoni-Freddari, C. *J. Cell Biol.* **1981**, *90*, 769.
(16) Adam-Vizi, V. *J. Neurochem.* **1992**, *58*, 395−405.
(17) Turner, D.; Stuenkel, E. L. *Neuroscience* **1998**, *86*, 547−556.
(18) Agarwal, R.; Iezhitsa, l.; Agarwal, P. *BioMetals* **2014**, *27*, 5−18.
(19) Dexter, D. T.; Wells, F. R.; Lee, A. J.; Agid, F.; Agid, Y.; Jenner, P.; Marsden, C. D. *J. Neurochem.* **1989**, *52*, 1830−1836.
(20) Crouch, P. J.; Barnham, K. J. *Acc. Chem. Res.* **2012**, *45*, 1604−1611.
(21) Zündorf, G.; Reiser, G. *Antioxid. Redox Signaling* **2011**, *14*, 1275−1288.
(22) Mueller, L.; Traub, H.; Jakubowski, N.; Drescher, D.; Baranov, V. I.; Kneipp, J. *Anal. Bioanal. Chem.* **2014**, *406*, 6963−6977.
(23) Liu, R.; Zhang, S.; Wei, C.; Xing, Z.; Zhang, S.; Zhang, X. *Acc. Chem. Res.* **2016**, *49*, 775−783.
(24) Trouillon, R.; Passarelli, M. K.; Wang, J.; Kurczy, M. E.; Ewing, A. G. *Anal. Chem.* **2013**, *85*, 522−542.
(25) Ortega, R.; Fayard, B.; Salomé, M.; Devès, G.; Susini, J. *Chem. Res. Toxicol.* **2005**, *18*, 1512−1519.
(26) Lin, Y.; Trouillon, R.; Safina, G.; Ewing, A. G. *Anal. Chem.* **2011**, *83*, 4369−4392.
(27) Tsang, C.-N.; Ho, K.-S.; Sun, H.; Chan, W.-T. *J. Am. Chem. Soc.* **2011**, *133*, 7355−7357.
(28) Gao, Y.; Lin, Y.; Zhang, B.; Zou, D.; He, M.; Dong, B.; Hang, W.; Huang, B. *Anal. Chem.* **2013**, *85*, 4268−4272.
(29) Lagerholm, B. C.; Wang, M.; Ernst, L. A.; Ly, D. H.; Liu, H.; Bruchez, M. P.; Waggoner, A. S. *Nano Lett.* **2004**, *4*, 2019−2022.
(30) Chang, C. J.; Jaworski, J.; Nolan, E. M.; Sheng, M.; Lippard, S. J. *Proc. Natl. Acad. Sci. U. S. A.* **2004**, *101*, 1129−1134.
(31) Li, L.; Li, P.; Fang, J.; Li, Q.; Xiao, H.; Zhou, H.; Tang, B. *Anal. Chem.* **2015**, *87*, 6057−6063.
(32) Li, Q.; Chen, P.; Fan, Y.; Wang, X.; Xu, K.; Li, L.; Tang, B. *Anal. Chem.* **2016**, *88*, 8610−8616.
(33) Li, X.; Hu, H.; Zhao, S.; Liu, Y.-M. *Anal. Chem.* **2016**, *88*, 5338−5344.
(34) Ino, K.; Okochi, M.; Konishi, N.; Nakatochi, M.; Imai, R.; Shikida, M.; Ito, A.; Honda, H. *Lab Chip* **2008**, *8*, 134−142.
(35) Dishinger, J. F.; Kennedy, R. T. *Anal. Chem.* **2007**, *79*, 947−954.
(36) Dittrich, P. S.; Tachikawa, K.; Manz, A. *Anal. Chem.* **2006**, *78*, 3887−3908.
(37) Kimmerling, R. J.; Lee Szeto, G.; Li, J. W.; Genshaft, A. S.; Kazer, S. W.; Payer, K. R.; de Riba Borrajo, J.; Blainey, P. C.; Irvine, D. J.; Shalek, A. K.; Manalis, S. R. *Nat. Commun.* **2016**, *7*, 10220.
(38) Krone, K. M.; Warias, R.; Ritter, C.; Li, A.; Acevedo-Rocha, C. G.; Reetz, M. T.; Belder, D. *J. Am. Chem. Soc.* **2016**, *138*, 2102−2105.
(39) Li, M.; Howson, S. E.; Dong, K.; Gao, N.; Ren, J.; Scott, P.; Qu, X. *J. Am. Chem. Soc.* **2014**, *136*, 11655−11663.
(40) Li, L.; Li, Q.; Chen, P.; Li, Z.; Chen, Z.; Tang, B. *Anal. Chem.* **2016**, *88*, 930−936.
(41) Kiemer, A. K.; Vollmar, A. M. *Immunol. Cell Biol.* **2001**, *79*, 11−17.
(42) Lee, S.; Lee, H. G.; Kang, S. H. *Anal. Chem.* **2009**, *81*, 538−542.
(43) Wulff, H.; Zhorov, B. S. *Chem. Rev.* **2008**, *108*, 1744−1773.
(44) Starikova, A. M.; Chvanov, M. A.; Pogorelaya, N. C.; Kostyuk, P. G. *Neuroscience* **1998**, *86*, 611−617.
(45) Lawson, K. *Kidney Int.* **2000**, *57*, 838−845.
(46) Grover, G. J.; McCullough, J. R.; Henry, D. E.; Conder, M. L.; Sleph, P. G. *J. Pharmacol. Exp. Ther.* **1989**, *251*, 98.
(47) Kong, X.; Su, F.; Zhang, L.; Yaron, J.; Lee, F.; Shi, Z.; Tian, Y.; Meldrum, D. R. *Angew. Chem., Int. Ed.* **2015**, *54*, 12053−12057.
(48) Wang, Y.; Mao, H.; Wong, L. B. *Talanta* **2011**, *85*, 694−700.
(49) Komatsu, H.; Iwasawa, N.; Citterio, D.; Suzuki, Y.; Kubota, T.; Tokuno, K.; Kitamura, Y.; Oka, K.; Suzuki, K. *J. Am. Chem. Soc.* **2004**, *126*, 16353−16360.
(50) Pandiella-Alonso, A.; Malgaroli, A.; Vicentini, L. M.; Meldolesi, J. *FEBS Lett.* **1986**, *208*, 48−51.
(51) Li, H.; Zhang, P.; Smaga, L. P.; Hoffman, R. A.; Chan, J. *J. Am. Chem. Soc.* **2015**, *137*, 15628−15631.
(52) Iadecola, C. *Nat. Rev. Neurosci.* **2004**, *5*, 347−360.
(53) Wang, G.; Krishnamurthy, K.; Tangpisuthipongsa, D. *J. Neurochem.* **2011**, *117*, 703−711.
(54) Varadarajan, S.; Kanski, J.; Aksenova, M.; Lauderback, C.; Butterfield, D. A. *J. Am. Chem. Soc.* **2001**, *123*, 5625−5631.
(55) Morth, J. P.; Pedersen, B. P.; Buch-Pedersen, M. J.; Andersen, J. P.; Vilsen, B.; Palmgren, M. G.; Nissen, P. *Nat. Rev. Mol. Cell Biol.* **2011**, *12*, 60−70.
(56) Bortner, C. D.; Sifre, M. I.; Cidlowski, J. A. *J. Biol. Chem.* **2008**, *283*, 7219−7229.
(57) Bortner, C. D.; Cidlowski, J. A. *J. Biol. Chem.* **2003**, *278*, 39176−39184.
(58) Arispe, N.; Rojas, E.; Pollard, H. B. *Proc. Natl. Acad. Sci. U. S. A.* **1993**, *90*, 567−571.
(59) Arispe, N.; Diaz, J.; Durell, S. R.; Shafrir, Y.; Guy, H. R. *Biochemistry* **2010**, *49*, 7847−7853.
(60) Adachi, M.; Nara, Y.; Mano, M.; Ikeda, K.; Horie, R.; Yamori, Y. *Clin. Exp. Pharmacol. Physiol.* **1993**, *20*, 587−593.
(61) Touyz, R. M.; Laurant, P.; Schiffrin, E. L. *J. Pharmacol. Exp. Ther.* **1998**, *284*, 998.

DOI: 10.1021/acs.analchem.6b05045
Anal. Chem. 2017, 89, 4559−4565